Femtosecond quantum optics with semiconductor nanostructures: single cycles of light, electrons and photons

A. Leitenstorfer*, R. Huber, R. Bratschitsch
University of Konstanz and Center for Applied Photonics, D-78457 Konstanz, Germany

ABSTRACT

Recent advances of femtosecond semiconductor physics at the limits of single electrons and photons down to sub-cycle time scales are presented. The first part deals with ultrafast measurements on single-electron systems: The transient quantum dynamics in a single CdSe/ZnSe quantum dot is investigated via femtosecond transmission spectroscopy. A two-color Er:fiber laser with excellent noise performance is key to these first resonant pump-probe measurements on a single-electron system. We have observed ultrafast bleaching of an electronic transition in a single quantum dot due to instantaneous Coulomb renormalization. Since we were also able to invert the two-level system, optical gain due to a single electron has been detected. By using π-pulses for probing, we could deterministically add or remove a single photon to or from a femtosecond light pulse, leading to non-classical states of the light field. In order to optimize electron-photon coupling, nanophotonic concepts like dielectric microresonators and metal optical antennas are explored. In the second part of the paper, we present multi-terahertz measurements on low-energy excitations in semiconductors. These studies lead towards a future time-domain quantum optics on a time scale of single cycles of light: Intense multi-terahertz fields of order MV/cm are used to coherently promote optically dark and dense para excitons in Cu_2O from the 1s into the 2p state. The nonlinear field response of the intra-excitonic degrees of freedom is directly monitored in the time domain via ultrabroadband electro-optic sampling. The experimental results are analyzed with a microscopic many-body theory, identifying up to two internal Rabi cycles. Subsequently, intersubband cavity polaritons in a quantum well waveguide structure are optically generated within less than one cycle of light by a femtosecond near-infrared pulse. Mid-infrared probe transients trace the non-adiabatic switch-on of ultrastrong light-matter coupling and the conversion of bare photons into cavity polaritons directly in the time domain.

Keywords: semiconductor quantum structures, femtosecond and terahertz spectroscopy, solid-state quantum optics

1. FEMTOSECOND NANO-OPTICS WITH SINGLE ELECTRON QUANTUM SYSTEMS

1.1 Two-color femtosecond pump-probe experiment on a single semiconductor quantum dot

Semiconductor quantum dots exhibit a discrete electronic level structure due to three-dimensional quantum confinement. They have been used as single-photon emitters, as well as non-classical current sources. Spin and charge degrees of freedom are hot candidates for solid-state quantum information processing. However, ensembles of quantum dots suffer inhomogeneous broadening. Therefore, the best insight into their physical properties and functionalities is gained studying single specimens. Most optical studies on single quantum dots are based on the detection of spontaneous emission of photons. This process typically occurs on time scales longer than 100 ps. In contrast, transient absorption experiments with ultrashort laser pulses provide high temporal resolution. Carrying out such experiments on single quantum systems is difficult since single-photon signals have to be filtered from an intense background.

*alfred.leitenstorfer@uni-konstanz.de; phone +49 7531 88-3818; fax +49 7531 88-3072;
www.uni-konstanz.de/quantum-electronics

Ultrafast Phenomena in Semiconductors and Nanostructure Materials XIV, edited by
Jin-Joo Song, Kong-Thon Tsen, Markus Betz, Abdulhakem Y. Elezzabi, Proc. of SPIE
Vol. 7600, 760002 · © 2010 SPIE · CCC code: 0277-786X/10/$18 · doi: 10.1117/12.847159

We present femtosecond transient transmission measurements on a single quantum dot with large confinement potential[1]. We use a 700 fs pump pulse to resonantly excite the self-assembled CdSe/ZnSe quantum system via a transition in the p-shell at a photon energy of 2.21 eV (Fig. 1). One electron-hole pair is generated by a pump with pulse area π.

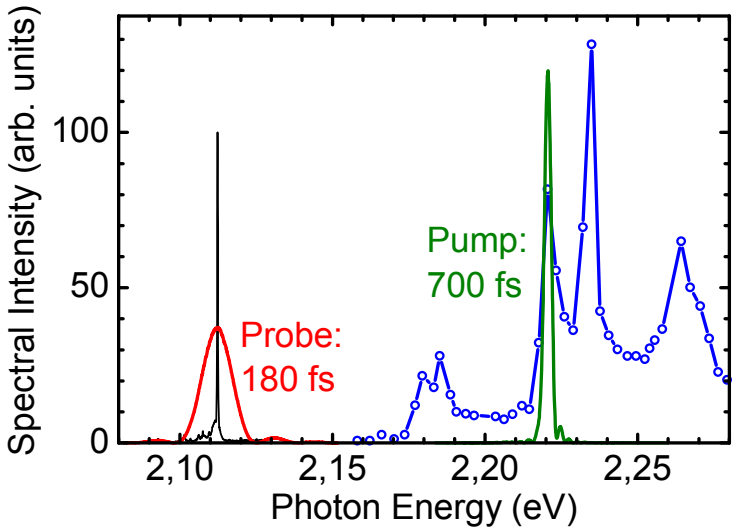

Figure 1. Photoluminescence and photoluminescence excitation spectra from a singly-charged CdSe/ZnSe quantum dot. The black line shows the luminescence emission intensity (X^- PL) as a function of photon energy. A photoluminescence excitation spectrum (X^- PLE) is given by the blue graph and provides information on electron-hole pair excitations with higher excess energy. The spectral envelopes of the pump and probe pulses provided by the two-color femtosecond fiber laser are depicted by the green and red lines, respectively.

We investigate a quantum dot that is already charged with one electron. As a consequence, an excited electron-hole pair forms a three-particle state. The transmission change induced by the pump excitation is measured as a function of delay time t_D with a 180 fs probe pulse resonant to the fundamental trion transition X^- at 2.11 eV. Our experiments are based on a fs-Er:fiber laser system that emits two independently tunable pulse trains with a relative timing jitter as low as 43 attoseconds at a repetition rate of 100 MHz[2,3]. To optimize the interaction of the probe photons with the single-electron system, the quantum dot is located in the optical near-field of a metallic nanoaperture. Energy information is obtained by spectrally dispersing the broadband probe beam transmitted through the sample with a monochromator of a resolution set to 200 μeV. Time-averaged parallel readout of 10^3 spectral channels for the differential transmission is achieved by operating a CCD array in a lock-in mode at a modulation frequency of 30 Hz.

The differential transmission change $\Delta T/T$ at the fundamental trion resonance X^- is shown as a function of delay time t_D and probe photon energy in Fig. 2. At negative time delays, a weak signal is discernible starting considerably before t_D = 0 ps. A step-like increase in differential transmission occurs around zero time delay t_D = 0. A constant region in $\Delta T/T$ follows, which persists until t_D = +10 ps. After an additional increase in transmission change, the signal remains stationary again for delay times t_D > 20 ps.

To explain the phenomena found in Fig. 2, we focus on differential spectra for several fixed time delays t_D (Fig. 3). At t_D = -2 ps, the probe pulse precedes the pump. In this situation, the probe beam first creates a coherent polarization at the s-shell transition (Fig. 4a) which is damped with the dephasing time corresponding to the sharp X^- resonance. The pump-induced perturbation of this free induction decay results in distinct oscillations in the differential transmission spectrum which are symmetric to a positive peak centered at the fundamental trion resonance. This coherent phenomenon is well-known from spectrally resolved pump-probe measurements on narrow resonances. It proves that we are readily detecting femtosecond transmission signals from a strongly confined quantum dot. The lines in the upper panel of Fig. 3 represent fits to the data based on the optical Bloch equations. In the model, the duration of the laser pulses is taken from the

experiment, the onset of perturbation in the free induction decay is given by the time integral of the pump intensity and the dephasing time is set to 5 ps to match the finite spectral resolution of our setup.

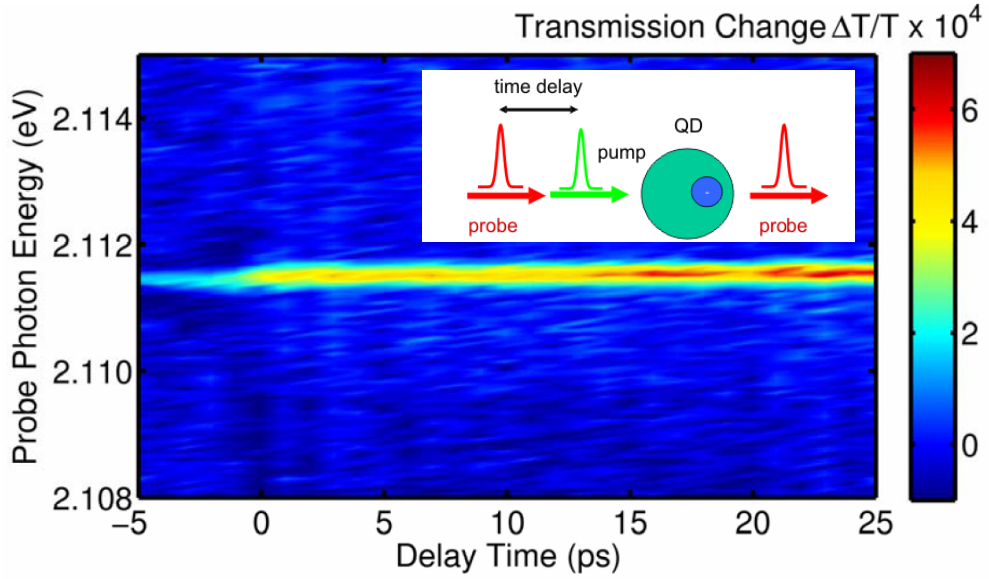

Figure 2. Differential transmission change $\Delta T/T$ at the fundamental trion resonance X^- color coded as a function of pump-probe delay time and probe photon energy. The probe pulse energy is kept in the linear regime. The pump pulse deterministically excites one electron-hole pair due to an area of π. Inset: schematic sketch explaining the time resolved transient transmission measurement.

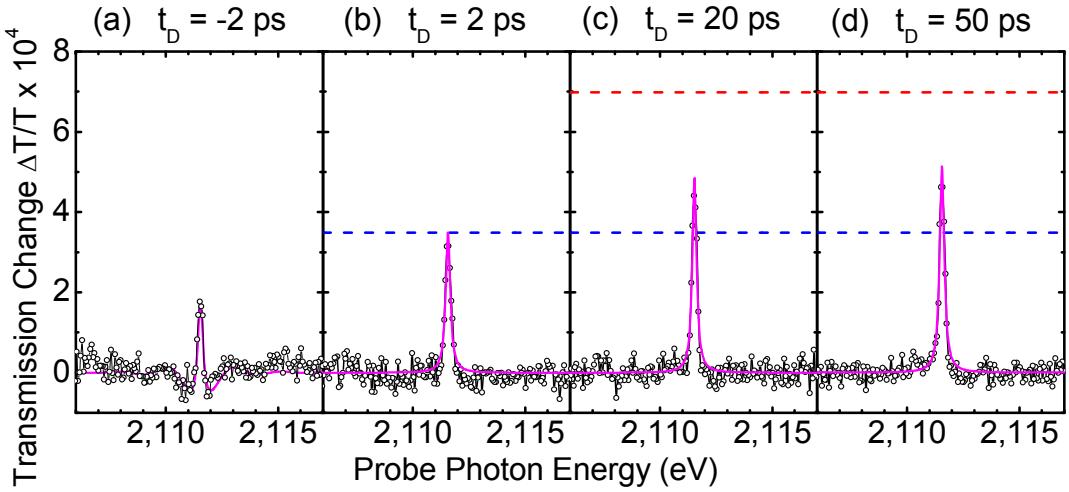

Figure 3. Spectrally resolved transmission changes as a function of probe photon energy and for different pump-probe time delays t_D. The experimental data are represented by the hollow circles, while fits based on the optical Bloch equations for a two-level system are given by the magenta lines. The lower dashed line (blue) marks the signal amplitude corresponding to pure bleaching of the X^- absorption found immediately after excitation. The upper dashed line (red) indicates the signal level expected for total inversion of the system.

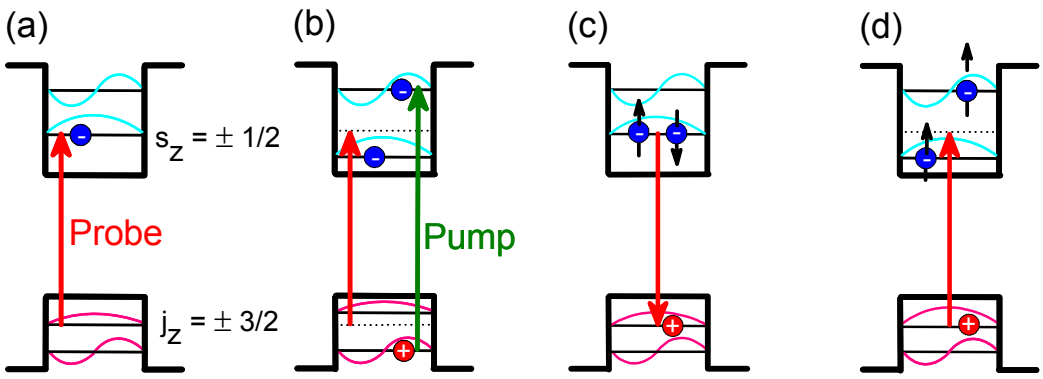

Figure 4. Schematic drawing of the electronic configurations relevant for the differential transmission signals during various stages in the excitation and relaxation process.

The differential transmission spectrum shortly after excitation is sampled at a delay time of +2 ps (Fig. 3b). In this case, we find a transmission increase with a Lorentzian line shape. The instantaneous onset around $t_D = 0$ is explained as follows: When the pump pulse creates an electron-hole pair in the p-shell (Fig. 4b), the charge distribution in the dot is altered. Due to the small dielectric constant of II-VI semiconductors, the resulting Coulomb force strongly renormalizes the electronic states. As a consequence, the original trion resonance vanishes and the probe beam suffers no more absorption. Our experiment measures the differential transmission change $\Delta T/T = (T_{pump\_on} - T_{pump\_off})/T$. Therefore, we observe a maximum at the fundamental trion transition.

The signal at the beginning of the second plateau in $\Delta T/T$ is probed at $t_D = +20$ ps (Fig. 3c). The delayed increase in differential transmission after the instantaneous Coulomb bleaching is due to energy relaxation of the hot electron-hole pair into the s-shell of the quantum dot: If the carriers excited into the p-shell have reached the lowest states in the potential wells (Fig. 4c), the fundamental trion resonance X^- is restored, but now under inversion conditions. When the probe pulse arrives at the system, it experiences optical gain due to stimulated emission.

The absolute amplitude of the differential transmission signal that we measure in the plateau at $t_D > 20$ ps is surprising: Assuming complete intraband relaxation and negligible interband recombination, one would expect an increase of $\Delta T/T$ by a factor of 2, as compared to the pure bleaching signal immediately after excitation. Instead, the observed increase saturates at a factor of exactly 1.5 for delay times between $t_D = 20$ ps and 50 ps (Fig. 3c and d). This finding indicates that inversion at the trion resonance and optical gain are established on a 15 ps time scale only after 50% of the pump pulses. This effect is due to the electron spin: There is equal probability for parallel and antiparallel relative alignment of the spins of the electron resident in the dot due to doping and the photoexcited electron since no magnetic field is applied to the sample. If the two electron spins are antiparallel, they are allowed to occupy the same spatial wave function in the s-shell of the potential well (Fig. 4c). Relaxation into the trion ground state proceeds quickly. If the two spins are parallel (Fig. 4d) relaxation of the photoexcited electron into the s-shell is forbidden by the Pauli exclusion principle. In our system, the only degree of freedom available to flip the electron spin from $s_z = -1/2$ to $s_z = +1/2$ is a Coulomb collision promoting the hole from its heavy hole ground state with total angular momentum projection $j_z = \pm 3/2$ into a light hole state with $j_z = \pm 1/2$. In order to fulfill energy and momentum conservation, a phonon scattering event of at least second order has to occur simultaneously. Obviously, this process occurs on a time scale much longer than 50 ps. Indeed, only after $t_D = 100$ ps, $\Delta T/T$ starts to decrease slowly because of the interband recombination time of the fundamental trion state of $\tau_{rad} = 480$ ps as measured by a time-resolved photoluminescence experiment.

The data in Figs. 2 and 3 have been obtained with weak probe pulses in the linear regime. If we increase the probe pulse area to π, exactly one photon should be absorbed from the 180 femtosecond probe pulse if it passes the quantum dot in its ground state. Furthermore, exactly one photon is added to the femtosecond pulse if it hits the system in the fundamental trion state. We can switch between both situations on a time scale as fast as 20 ps, while no interaction with the system would occur in the intermediate time interval due to Coulomb renormalization. To start exploring the physics of coherent single photon gain triggered by ultrashort light pulses, we have performed the following experiment: we

measure the differential transmission at t_D = 20 ps for increasing average powers of the probe beam starting at P_{probe} = 75 μW (Fig. 5a). In this case, the pulse area amounts to 0.3 π. We assume that the quantum dot is initially in the inverted state |X⁻>. The Bloch vector of the two-level system is then turned downwards by an angle of 0.3 π, creating a considerable amount of interband polarization. In Fig. 5a we plot the temporal envelope of the probe electric field (blue line) and of the polarization amplitude (green line) derived from the optical Bloch equations. Starting at |X⁻>, the electric field reemitted by the polarization of the inverted transition interferes constructively with the probe and creates a positive peak in the differential transmission spectrum. This signal appears in both the experimental data (circles in Fig. 5a), as well as in the simulated differential transmission spectrum (magenta line). In Fig. 5b, we further increase P_{probe} to 400 μW, which corresponds to a pulse area of 0.7 π. The polarization (green line) now experiences a maximum during the probe pulse. The polarization exhibits a tail which is similar in amplitude as after the 0.3 π pulse of Fig. 5a. However, the probe electric field has been increased substantially at 0.7 π compared to 0.3 π (blue line in Fig. 5b). For this reason, the coherent two-level model yields a decrease in peak amplitude for the relative transmission change $\Delta T/T$ (magenta line in Fig. 5(b)). In addition, a positive background signal extending over the entire probe bandwidth starts to develop, corresponding to the normalized Fourier transform of the fast initial peak in the polarization response.

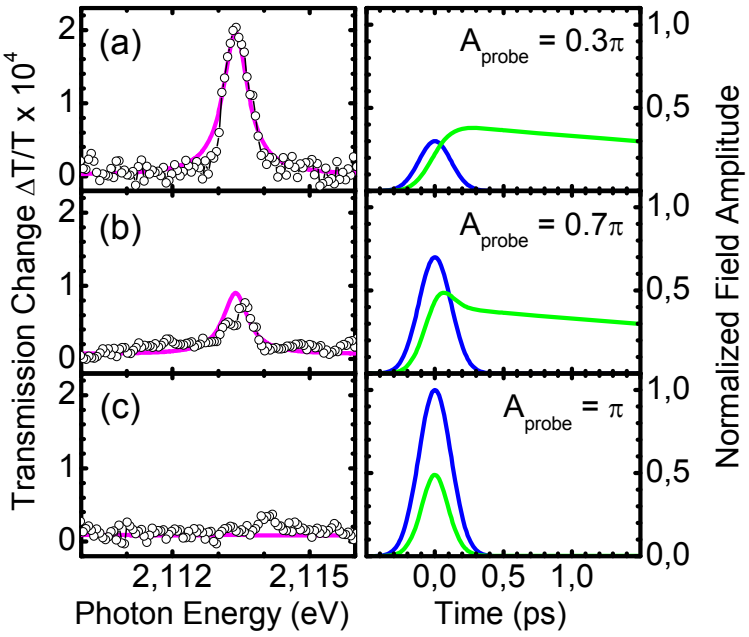

Figure 5. Spectral transmission change $\Delta T/T$ measured at a delay time of t_D = 20 ps. Average powers of the probe beam P_{probe} are increased beyond the linear regime. Experimental data are represented by hollow circles on the left hand side. The magenta lines represent differential transmission spectra calculated via the optical Bloch equations. The temporal envelopes of the probe electric field (blue lines) and the electron-hole polarization (green lines) are depicted on the right hand side of a-c for increasing probe pulse area A_{probe}.

The most interesting situation is encountered when P_{probe} is further increased to 800 μW, yielding a probe pulse area of π (see Fig. 5c). Such a light pulse coherently drives the quantum system from the eigenstate |X⁻> back to the ground state |e>. The polarization induced by the probe pulse lacks a tail and follows closely the temporal envelope of the probe electric field (see green and blue graphs in Fig. 5(c)). In this situation exactly one photon is added to the probe pulse by a narrow resonance, but it does not change the shape of the temporal and spectral envelope of the femtosecond light pulse that gets amplified. As a result, the model predicts a flat but slightly positive differential transmission spectrum which is in good agreement with the $\Delta T/T$ we record experimentally (magenta graph and circles in Fig. 5c). Due to the inherent nonlinearity of the two-level system its polarization response to a short and broadband pulse is different to the coherent

sum of the isolated responses induced by its narrow-band Fourier components. Spectral analysis of the probe after transmission through the quantum system yields information about the temporal structure of the single-photon gain: An isolated peak at X^- indicates that radiation is triggered linearly into the picosecond polarization decay (Fig. 5a). The positive broadband signal in Fig. 5c corresponds to deterministic single-photon emission within a time window set by the 180 fs probe. The ratio between the spectral weight of the narrowband resonance and the broadband background found together in Fig. 5b measures the admixture of both limiting cases. The features we observe in the nonlinear probing regime are intrinsic to coherent light-matter interaction and beyond the validity of rate equation models for stimulated emission.

1.2 Towards femtosecond control of single electrons with single photons and vice versa

In our present experiment, approximately 10000 transmitted photons per pulse are necessary to read out the X^- resonance. Therefore, the influence of our femtosecond single photon absorber and amplifier on the quantum statistics of the probe field is limited. The enhancement of the interaction between quantum dot and electromagnetic field might lead to a situation, where single photons can be deterministically added to or subtracted from transients containing single or few quanta of light. Such ultrafast manipulation of pulses with well-defined photon number could enable a new class of quantum optics experiments and offer possibilities for quantum information processing at terahertz clock rates. An enhanced interaction of the light field and the single quantum dot may be envisioned by positioning a single quantum dot in the gap of a broadband optical antenna[4,5] (Fig. 6a) and/or inside a dielectric microcavity[6,7] (Fig. 6b).

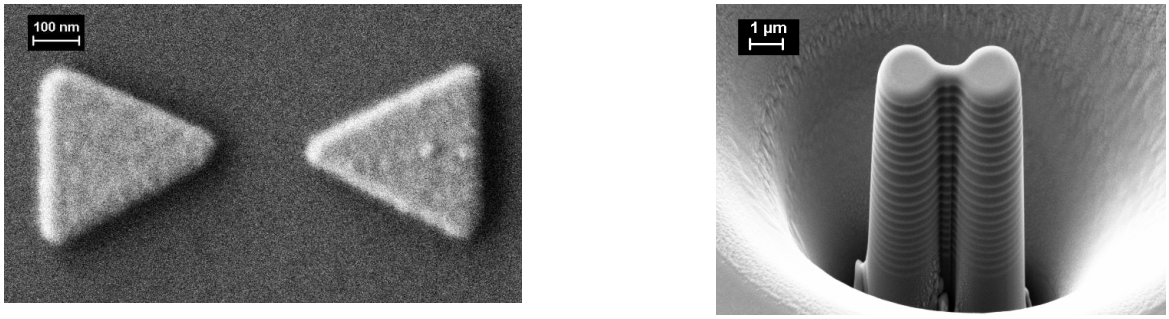

Figure 6. Scanning electron micrograph of a metal nanoantenna (a) and two coupled dielectric microcavities (b).

2. TERAHERTZ QUANTUM OPTICS ON THE SUB-CYCLE SCALE: FROM EXCITONS TO ULTRASTRONG LIGHT-MATTER COUPLING

A second exciting avenue of femtosecond quantum optics has been opened up by the recent progress of ultrabroadband terahertz (THz) technology: Techniques such as optical rectification and electro-optic detection have afforded full access to both amplitude and phase of electromagnetic fields, in the time domain[8-11]. While these possibilities started out in the far infrared, the accessible bandwidth of phase-locked pulse synthesis and field-sensitive detection has been vastly increased to approach the near infrared, lately[9,10]. Equally important, the efficiency of THz sources has been dramatically improved within the last year to reach peak fields in excess of 100 MV/cm - surpassing even typical intra-atomic fields[11]. State-of-the-art THz photonics has made it possible to trace ultrafast dynamics[12-16] and to drive first strong nonlinearities with a time resolution better than a single oscillation cycle of light[11,17,18]. In the following two sub-sections, we discuss lead-off quantum optics experiments which explore this new field[17,19].

2.1 Terahertz Coherent Control of the Internal Quantum State of Dark Excitons in Cu_2O

When Bose-Einstein condensation (BEC) of atomic gases was first demonstrated, a sophisticated arsenal of quantum optical protocols had been at hand. Excitons have been discussed as another potential candidate for BEC. Yet coherent control of promising excitons for BEC by conventional optical techniques has been a challenge since relevant systems typically exhibit weak if any radiative interband coupling. 1s para-excitons in Cu_2O are a prominent example. Terahertz (THz) pulses, in contrast, couple resonantly to the internal atom-like fine structure, irrespective of interband selection rules. This approach has provided novel insight into the formation, fine structure, density, and temperature of excitons[15,20]. The observation of stimulated THz emission from intra-excitonic transitions[21] has raised the hope for future coherent manipulation of dark exciton ensembles similar to atomic quantum optics.

We employ intense THz transients to coherently control the internal quantum state of optically dark, dense, and cold 1s-para excitons in Cu_2O, for the first time. The sample is a naturally grown single crystal of Cu_2O (thickness: 334 μm) kept at a lattice temperature of $T_L = 4$ K. Near infrared femtosecond pulses centered at a photon energy of 1.5 eV are absorbed via two-photon transitions to generate unbound electron-hole pairs with homogeneous density throughout the crystal length.

In a first set of experiments, we monitor the formation and cooling dynamics of 1s excitons via time-delayed multi-THz transients probing the internal 1s-2p absorption. Strong exchange interaction splits the $n = 1$ state into a triplet ortho-exciton and a lower-lying, optically inaccessible singlet para-exciton. The corresponding 1s-2p Lyman lines are located at photon energies of 116 meV and 129 meV, respectively. Fig. 7a depicts the pump-induced absorption changes in this frequency window for various delay times t_D after photogeneration of e-h pairs. While the spectrally broad THz absorption at early delay times is indicative of unbound e-h pairs, the hallmark 1s-2p absorption lines are already visible at $t_D = 11$ ps. Within 100 ps, the lines narrow down and shift slightly towards lower frequencies. Simultaneously, the ratio of para- versus ortho-exciton absorption increases over time. The subsequent decay of the exciton population follows a complex non-exponential dynamics (not shown).

With the internal dipole moments known from Ref. 21, the strength of THz absorption is an absolute measure of the densities $N_{1s,para}$ and $N_{1s,ortho}$. Due to their very different effective masses the energetic distance of 1s and 2p excitons increases with larger center-of-mass momenta, and the temperature T_{1s} is encoded in the THz line shape. For $t_D = 100$ ps (see dots in Fig. 7a), we find best agreement with the experiment for values as high as $N_{1s,para} = 1 \times 10^{16}$ cm^{-3} and $N_{1s,\,ortho} = 5 \times 10^{15}$ cm^{-3}, and a temperature $T_{1s} = 10$ K close to the phonon bath. $N_{1s,para}$ is thus only one order of magnitude below critical values for potential BEC.

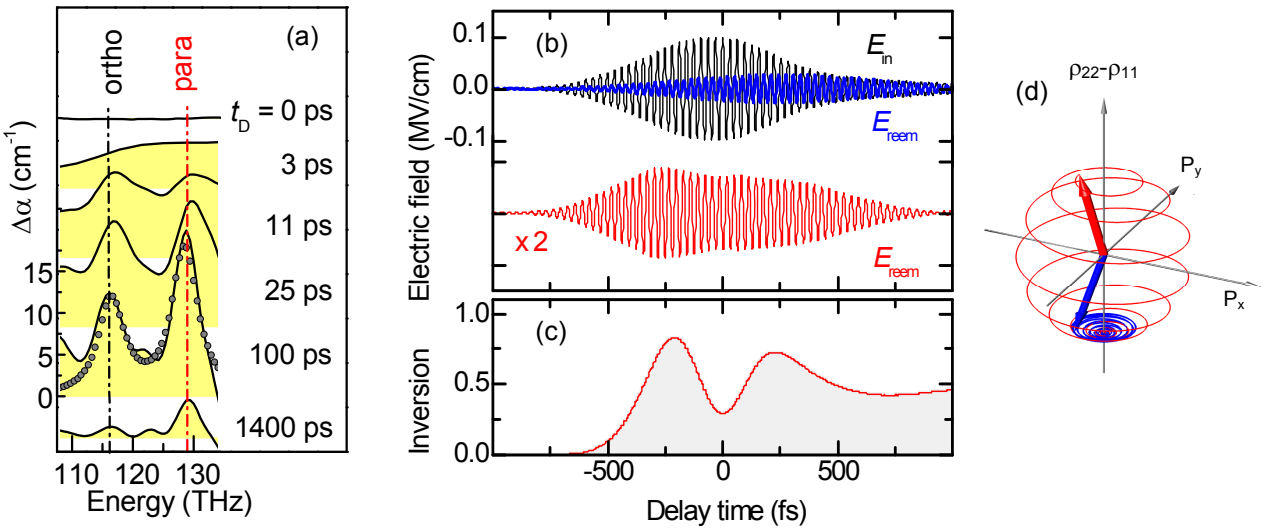

Figure 7. (a) Ultrafast formation and cooling dynamics of 1s excitons in bulk Cu_2O (T_L = 4 K): Pump-induced changes $\Delta\alpha$ of the mid-infrared absorption for various delay times t_D after two-photon absorption of 12-fs near-infrared pulses (λ_{center} = 800 nm). Energy positions of the intra-excitonic 1s-2p resonances in the ortho and para system at vanishing center-of-mass momentum are indicated by vertical lines. Circles: Numerical fit of the line shapes with parameters (see text) $N_{1s,para} = 1 \times 10^{16}$ cm^{-3}, $N_{1s,ortho} = 5 \times 10^{15}$ cm^{-3}, T_{1s} = 10 K. (b) THz transient resonantly driving the atom-like internal 1s-2p transition of paraexcitons in Cu_2O (upper curve). The reemitted field (lower curve) exhibits a non-monotonous envelope characteristic of up to two internal Rabi cycles. (c) A microscopic theory confirms an oscillatory change of the population inversion of the 1s-2p two-level system. (d) Schematic of the Bloch sphere of the 1s-2p intra-excitonic two-level system.

We next demonstrate how to control the internal quantum state of the dark, dense, and cold para-exciton gas formed at t_D = 400 ps. To this end, intense THz transients are generated via optical rectification of the output of a high-power Ti:sapphire laser amplifier in a GaSe emitter of a thickness of 200 μm. The black line in Fig. 7b depicts a THz pulse of moderate intensity (E_{peak} = 0.1 MV/cm) on resonance with the two-level system consisting of the 1s- and 2p-para states. The oscillating reemitted field is directly measured by electro-optic detection, on a femtosecond scale (blue curve). The phase of the transient is shifted by approximately π with respect to the driving field - characteristic of an absorptive transition in a resonant two-level system. The free induction decay following the external THz pulse exhibits a decoherence time of 0.7 ps. This response is compared with the polarization induced by a THz pulse of the same temporal profile, but a peak electric field increased by a factor of 5 (see red curve, Fig. 7b). Surprisingly, the transient is not an upscaled version of the low-field response. Rather, the field rises more rapidly, reaches its maximum before the peak of the pump transient, and decreases within the coherence window. Also, the maximum value of the amplitude saturates for increasing excitation density. Most remarkably, the curve exhibits a structured envelope with two maxima. The onset of an oscillatory behaviour indicates that the intense THz beam leads to nonlinear dynamics of dark exciton populations well beyond the perturbative regime.

To first approximation, the dynamics is a manifestation of a partial Rabi oscillation well understood in a Bloch picture of the two-level system (see Fig. 7d). Here, the diagonal (population difference ρ_{22}-ρ_{11}) and off-diagonal (polarizations P_x and P_y) elements of the density matrix are depicted as the vertical and the two horizontal coordinates. For low driving fields, the Bloch vector performs a Larmor precession in the vicinity of the south pole of the Bloch sphere. Experimentally, the projection of this trajectory onto the polarization axis is directly mapped out in real time (Fig. 7b). With increasing THz field, the state vector may be driven towards the north pole inducing strong population inversion. During this partial Rabi cycle, the projection onto the polarization axis reaches a maximum at the equator and decreases from there on. The real time data of the polarization directly reflect this dynamics (Fig. 7c) and allow us to reconstruct the actual motion of the Bloch vector. From a comparison of the data with a microscopic description of intraexcitonic

light-matter coupling and dynamics[22], we find that up to 80% of the optically dark states are promoted from the 1s into the 2p orbital.

Our results point out a promising route towards systematic quantum optics with optically dark excitons. In the future, advanced protocols known from atomic systems may open new perspectives for preparing ultracold and dense exciton gases using high-field THz transients.

2.2 Switch-on of Ultrastrong Light-Matter Interaction within Less than a Single Cycle of Light

Sub-cycle resolution unfolds a particularly fascinating power in the field of cavity quantum electrodynamics (cavity-QED): In the strong coupling regime, a photon enclosed in microcavity may be absorbed and spontaneously reemitted by an elementary excitation many times before dissipation becomes effective. This process gives rise to new eigenstates of mixed light-matter character, so-called cavity polaritons. These excitations display an energy anticrossing known as vacuum-field Rabi splitting Ω_R [23]. Recently intersubband resonances of semiconductor quantum wells (QW) coupled to the mid-infrared photon mode of a planar waveguide have entered a new regime of ultrastrong interaction, where Ω_R amounts to a significant fraction of the bare eigenfrequencies ω_{12} themselves[24]. The resulting squeezed two-mode quantum vacuum is expected to give rise to a variety of novel QED effects[25]. In particular, ultrafast non-adiabatic switching of the Rabi frequency Ω_R has been predicted to release correlated photon pairs out of the vacuum, reminiscent of the intriguing, yet unobserved dynamic Casimir effect[25].

Up to now, however, non-adiabatic phenomena – classical or QED in nature – remained an academic curiosity since there has been no laboratory capable of controlling light-matter interaction on a sub-cycle scale. While electronic means offer a versatile approach to control Ω_R, e.g. by an external gate voltage[26], such techniques are too slow to study the predicted QED phenomena. Here, we report an all-optical pump – multi-THz probe scheme for the first implementation of non-adiabatic control of ultrastrongly coupled cavity polaritons[19].

The sample contains 50 identical, undoped GaAs QWs separated by $Al_{0.33}Ga_{0.67}As$ barriers. The electronic wave functions are quantized along the growth direction forming subbands (Fig. 8). These are unpopulated in thermal equilibrium. Radiative transitions between subbands of quantum number n = 1 and n = 2 are activated if optical excitation promotes electrons from the valence into the conduction band. The intersubband resonance features a narrow absorption line centered about a photon energy of $\hbar\omega_{12}$ = 120 meV (wavelength λ = 10 μm) and a strong dipole moment oriented along the growth direction. The multi-QW structure is designed as a planar step index waveguide for mid-infrared light[24]. Radiation is confined between a top-cladding ($Al_{0.33}Ga_{0.67}As$)-air interface (n_{air} = 1, n_{QW} = 3.1) on one side and a low refractive index AlAs layer (n_{AlAs} = 2.9) on the other. The effective thickness of the entire waveguide is chosen to be $\lambda/2$ at an internal angle of θ = 65°. Photon modes with electric field components in growth direction (TM polarization) may resonantly couple to intersubband transitions provided the subbands are populated.

We employ a low-noise Ti:sapphire laser system generating amplified 12-fs pulses (central photon energy: 1.55 eV) to photoinject electrons from the valence band into the lowest conduction subband of the QWs (Fig. 8), activating the intersubband boson field. The subsequent ultrafast dynamics of the non-equilibrium cavity is traced by multi-THz spectroscopy[12-14]: A second part of the laser output generates phase-locked THz pulses covering the spectral window from 80 meV to 150 meV by optical rectification in a 50-μm-thin GaSe emitter[8]. TM polarized field transients are coupled through the prism-shaped substrate and internally reflected off the photoexcited area of the waveguide under incidence angles around θ = 65° (Fig. 8). The pulse front of the near-infrared pump is tilted to match the geometry of the THz phase surfaces. The oscillating electric field of the reflected THz transient is resolved in the time domain via phase-matched electro-optic sampling[8,9].

Fourier transformation provides amplitude (Fig. 9) and phase spectra in the mid infrared. The eigenmodes of the cavity are identified via their characteristic minima in the amplitude reflectivity[24]. We repeat the experiments for various delay times t_D between near-infrared pump and multi-THz probe pulses. For $t_D \leq$ -50 fs the spectra are dominated by a single dip at 113 meV. On resonance, the amplitude reflectivity drops below 10%. Since there is no material excitation in the equilibrium sample throughout the frequency window shown, the observed feature is unequivocally assigned to the photonic waveguide mode.

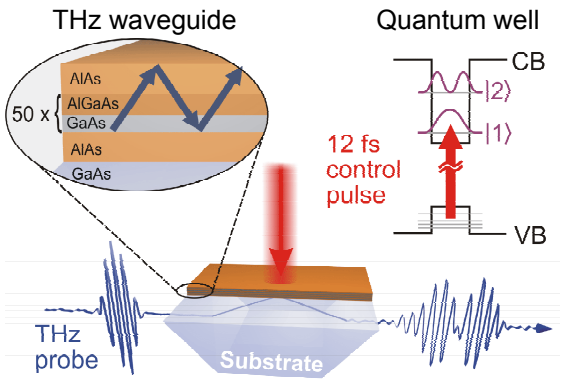

Figure 8. Schematic of the femtosecond optical switch: 50 undoped GaAs quantum wells (L = 9 nm) separated by $Al_{0.33}Ga_{0.67}As$ barriers are embedded into a planar waveguide based on total internal reflection. Intersubband transitions are activated by near infrared 12-fs control pulses populating level |1⟩. TM-polarized multi-THz transients guided through the prism-shaped substrate are reflected off the waveguide to probe the ultrafast buildup of intersubband cavity polaritons.

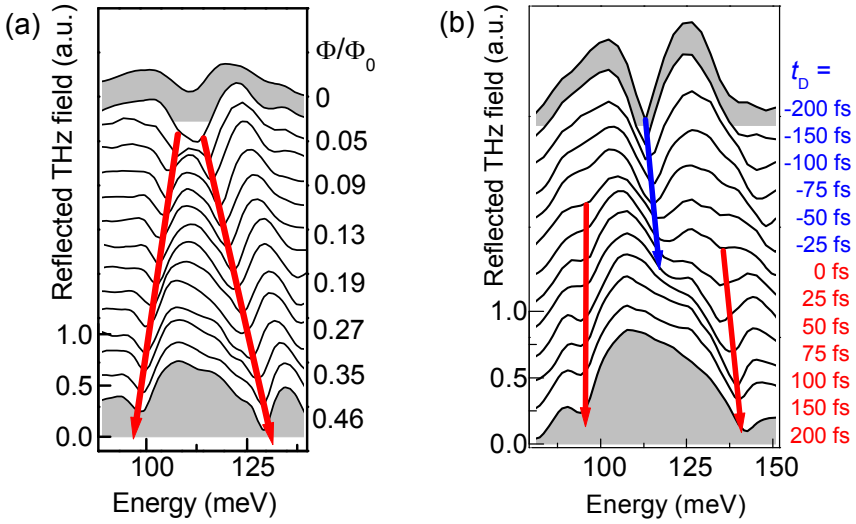

Figure 9. (a) THz reflectance spectra measured at room temperature for various control fluences Φ (t_D = 20 ps). Minima indicate eigenmodes. For Φ = 0, only the bare photon mode is observed; both cavity polariton branches are discernible for Φ ≥ 0.05 Φ_0 (Φ_0 = 0.1 mJ/cm^2). (b) THz reflectance spectra given for various delay times t_D reveal the non-adiabatic switch-on dynamics of ultrastrongly coupled cavity polaritons. The 12-fs control pulse (Φ = Φ_0) arrives at t_D = 0. Blue arrow: bare cavity resonance, red arrows: ultrastrongly coupled intersubband cavity polaritons.

Photoinjection of electrons into the lower subband induces dramatic changes of the spectra of order unity. The initial bare photon eigenstate is replaced, on a ten femtosecond scale, by two coupled cavity polariton modes appearing simultaneously at energies of 94 meV and 136 meV, respectively. Most remarkably, these new resonances do not gradually develop out of the bare cavity mode. Rather a discontinuous switching to a cavity polariton system is seen with our sub-cycle time resolution. A slight additional shift of both new resonances occurs within the subsequent window of 200 fs. The maximum polariton splitting amounts to as much as 50 meV, corresponding to a fraction of 44 % of the bare photon frequency. This value is comparable to the record achieved in delta-doped structures to date and clearly fulfills the criteria of ultrastrong light-matter coupling[25]. The vacuum Rabi frequency is continuously tuned via the near-infrared pump power (not shown).

Non-adiabatic switching of the light-matter Hamiltonian is predicted to give rise to yet unexplored effects on pre-existing photon states and the quantum vacuum itself[25]. In order to appreciate the impact of sub-cycle control, we prepare a coherent photon state in the bare cavity and perturb the radiative relaxation by non-adiabatic switching. On a sub-cycle scale, the photon population converts into ultrastrongly coupled coherent polaritons. Electro-optic sampling directly monitors this phenomenon for the first time (not shown). A quantitative theory including anti-resonant terms of the light-matter Hamiltonian as well as the extremely non-equilibrium carrier dynamics is currently under way.

In conclusion, we have demonstrated the first non-adiabatic switching scheme of cavity-polaritons, reaching the regime of ultrastrong light-matter coupling on a sub-cycle scale. The experiments provide a benchmark for latest theories in the ultrastrong coupling regime, point out a viable route towards novel QED phenomena such as the observation of Casimir-type vacuum radiation, and demonstrate an optical switching device at the ultimate speed.

REFERENCES

1. Sotier, F., Thomay, T., Hanke, T., Korger, J., Mahapatra, S., Frey, A., Brunner, K., Bratschitsch, R., and Leitenstorfer, A., "Femtosecond few-fermion dynamics and deterministic single-photon gain in a quantum dot," Nature Phys. 5, 352 (2009).
2. Moutzouris, K., Adler, F., Sotier, F., Träutlein, D., and Leitenstorfer, A., "Multimilliwatt ultrashort pulses continuously tunable in the visible from a compact fiber source," Opt. Lett. 31, 1148 (2006).
3. Adler, F., Sell, A., Sotier, F., Huber, R., and Leitenstorfer, A., "Attosecond relative timing jitter and 13 fs tunable pulses from a two-branch Er:fiber laser," Opt. Lett. 32, 35046 (2007).
4. Merlein, J., Kahl, M., Zuschlag, A., Sell, A., Halm, A., Boneberg, J., Leiderer, P., Leitenstorfer, A., and Bratschitsch, R., "Nanomechanical control of an optical antenna," Nature Phot. 2, 230 (2008).
5. Hanke, T., Krauß, G., Wild, B., Träutlein, D., Lohss, S., Bratschitsch, R., and Leitenstorfer A., "Efficient nonlinear light emission of single gold optical antennas driven by few-cycle near-infrared pulses," Phys. Rev. Lett. 103, 257404 (2009).
6. Kahl, M., Thomay, T., Kohnle, V., Beha, K., Merlein, J., Hagner, M., Halm, A., Ziegler, J., Nann, T., Fedutik, Y., Woggon, U., Artemyev, M., Pérez-Willard, F., Leitenstorfer, A., and Bratschitsch, R., "Colloidal quantum dots in all-dielectric high-Q pillar microcavities," Nano Lett. 7, 2897 (2007).
7. Thomay, T., Hanke, T., Tomas, M., Sotier, F., Beha, K., Knittel, V., Kahl, M., Whitaker, K. M., Gamelin, D. R., Leitenstorfer, A., and Bratschitsch, R., "Colloidal ZnO quantum dots in ultraviolet pillar microcavities," Opt. Express 16, 9791 (2008).
8. Huber, R., Brodschelm, A., Tauser, F., and Leitenstorfer, A., "Generation and field-resolved detection of femtosecond electromagnetic pulses tunable up to 41 THz," Appl. Phys. Lett. 76, 3191 (2000).
9. Kübler, C., Huber, R., Tübel, S., and Leitenstorfer, A., "Ultrabroadband detection of multi-terahertz field transients with GaSe electro-optic sensors: Approaching the near infrared," Appl. Phys. Lett. 85, 3360 (2004).
10. Sell, A., Scheu, R., Leitenstorfer, A., and Huber, R., "Field-resolved detection of phase-locked infrared transients from a compact Er:fiber system tunable between 55 and 107 THz," Appl. Phys. Lett. 93, 251107 (2008).
11. Sell, A., Leitenstorfer, A., and Huber, R., "Phase-locked generation and field-resolved detection of widely tunable terahertz pulses with amplitudes exceeding 100 MV/cm," Opt. Lett. 33, 2767 (2008).
12. Huber, R., Tauser, F., Brodschelm, A., Bichler, M., Abstreiter, G., and Leitenstorfer, A., "How many-particle interactions develop after ultrafast excitation of an electron-hole plasma," Nature 414, 286 (2001).
13. Huber, R., Kübler, C., Tübel, S., Leitenstorfer, A., Vu, Q.T., Haug, H., Köhler, F., and Amamm, M.-C., "Femtosecond Formation of Coupled Phonon-Plasmon Modes in InP: Ultrabroadband THz Experiment and Quantum Kinetic Theory," Phys. Rev. Lett. 94, 0274011 (2005).
14. Kübler, C., Ehrke, H., Huber, R., Lopez, R., Halabica, A., Haglund Jr., R.F., and Leitenstorfer, A., "Coherent Structural Dynamics and Electronic Correlations during an Ultrafast Insulator-to-Metal Phase Transition in VO_2," Phys. Rev. Lett. 99, 116401 (2007).
15. Kaindl, R.A., Carnahan, M.A., Hägele, D., Lövenich, R., and Chemla, D.S., "Ultrafast terahertz probes of transient conducting and insulating phases in an electron–hole gas," Nature 423, 734 (2003).
16. Kampfrath, T., Perfetti, L., Schnapper, F., Frischkorn, C., and Wolf, M., "Strongly Coupled Optical Phonons in the Ultrafast Dynamics of the Electronic Energy and Current Relaxation in Graphite," Phys. Rev. Lett. 95, 187403 (2005).

17. Leinß, S., Kampfrath, T., Volkmann, K.V., Wolf, M., Steiner, J.T., Kira, M., Koch, S.W., Leitenstorfer, A., and Huber, R., "Terahertz coherent control of optically dark paraexcitons in Cu_2O," Phys. Rev. Lett. 101, 246401 (2008).
18. Kampfrath, T., Sell, A., Klatt, G., Pashkin, A., Mährlein, S., Dekorsy, T., Wolf, M., Fiebig, M., Leitenstorfer, A., and Huber, R., "Ultrafast magnetic twist: How intense terahertz transients control spin waves coherently," submitted for publication (2009).
19. Günter, G., Anappara, A.A., Hees, J., Sell, A., Biasiol, G., Sorba, L., De Liberato, S., Ciuti, C., Tredicucci, A., Leitenstorfer, A., and Huber, R., "Sub-cycle switch-on of ultrastrong light-matter interaction," Nature 458, 178 (2009).
20. Huber, R., Kaindl, R.A., Schmid, B.A., and Chemla, D.S., "Broadband terahertz study of excitonic resonances in the high-density regime in GaAs/$Al_xGa_{1-x}As$ quantum wells," Phys. Rev. B Rapid 72, 161314(R) (2005).
21. Huber, R., Schmid, B.A., Shen, Y.-R., Chemla, D.S., and Kaindl, R.A., "Stimulated Terahertz Emission from Intraexcitonic Transitions in Cu_2O," Phys. Rev. Lett. 96, 017402 (2006).
22. Kira, M., Koch, S.W., "Many-body correlations and excitonic effects in semiconductor spectroscopy," Prog. Quant. Electron. 30, 155 (2006).
23. Weisbuch, C., Nishioka, M., Ishikawa, A., and Arakawa, Y., "Observation of the coupled exciton-photon mode splitting in a semiconductor quantum microcavity," Phys. Rev. Lett. 69, 3314 (1992).
24. Dini, D., R. Köhler, A. Tredicucci, G. Biasiol, and L. Sorba, "Microcavity Polariton Splitting of Intersubband Transitions," Phys. Rev. Lett. 90, 116401 (2003).
25. Ciuti, C., Bastard, G., and Carusotto, I., "Quantum vacuum properties of the intersubband cavity polariton field," Phys. Rev. B 72, 115303 (2005).
26. Anappara, A., Tredicucci, A., Biasiol, G., and Sorba, L., "Electrical control of polariton coupling in intersubband microcavities," Appl. Phys. Lett. 87, 051105 (2005); Anappara, A., De Liberato, S., Tredicucci, A., Ciuti, C., Biasiol, G., Sorba, L., and Beltram F., "Signatures of the ultrastrong light-matter coupling regime," Phys. Rev. B Rapid 79, 201303 (2009); Anappara, A., Tredicucci, A., Beltram, F., Biasiol, G., and Sorba, L., "Tunnel-assisted manipulation of intersubband polaritons in asymmetric coupled quantum wells," Appl. Phys. Lett. 89, 171109 (2006).